Experimental and Theoretical Performance of a Supercavitating Hydrofoil Operating near a Free Surface

J. O. Scherer* and J. Auslaender†
Hydronautics, Inc., Laurel, Md.

Results of lift and drag measurements performed on a 5-in. chord model of the BuShips parent hydrofoil are presented and compared with theoretical predictions. The tests were conducted in the high-speed, variable-pressure, free-surface, circulating water channel at Hydronautics, Inc. They cover angles of attack ranging from 3° to 15°, vapor cavitation numbers from 0.06 to 2.34, depths of submergence of ½ and 1 chord, and velocities from 30 to 52 fps. It is found that, at vapor cavitation numbers that are low enough to approach prototype values, the ventilation hysteresis is eliminated. Results are presented in the form of tables and graphs of lift and drag coefficients for variations of angle of attack and vapor cavitation numbers. Good agreement is found between theory and experiment. The problems of ventilation inception are also discussed.

Nomenclature

A = aspect ratio = $b^2/S = b/c$
b = foil span
BC = base ventilated flow with leading edge bottom vapor cavitation
BV = base ventilated flow with no vapor cavitation
c = mean chord length of foil
C_L = lift coefficient = $L/\frac{1}{2}\rho U_\infty^2 S$
C_D = drag coefficient = $D/\frac{1}{2}\rho U_\infty^2 S$
D = total drag of foil-strut combination
FV = fully ventilated flow
h = depth of submersion of foil leading edge
h_L = height of foil leading edge above channel floor
L = total lift of foil-strut combination
p_c = cavity pressure
p_v = vapor pressure of fluid
p_∞ = static pressure in freestream
S = projected area of foil
t = foil thickness = $y_c - y_0$
TC = base ventilated flow with leading edge top vapor cavitation
U_∞ = freestream velocity
y_c = ordinate of upper surface of hydrofoil with respect to reference line
y_0 = ordinate of lower surface of hydrofoil with respect to reference line
α_g = geometric angle of attack measured to nose-tail line of foil, corrected for channel wall effects
α_g' = geometric angle of attack measured to nose-tail line of foil, uncorrected for channel wall effects
σ_i = cavity cavitation number = $(p_\infty - p_c)/\frac{1}{2}\rho U_\infty^2$
σ_v = vapor cavitation number = $(p_\infty - p_v)/\frac{1}{2}\rho U_\infty^2$
ρ = mass density of fluid

Introduction

In 1961, Hydronautics, Inc. designed a low-drag supercavitating hydrofoil for the U. S. Navy Bureau of Ships. This foil, known as the BuShips parent supercavitating hydrofoil, was designed according to the linearized theory for supercavitating hydrofoils operating near a free surface[2–4] using the Tulin low-drag two-term camber distribution.[5] A 5-in. chord model was built by Grumman Aircraft for the Bureau of Ships and was tested in the high-speed, variable-pressure, free-surface water channel at Hydronautics, Inc. This facility is described in detail in Ref. 6.

In the present paper the results of tests of the BuShips parent foil without flaps are presented and compared with theory. The tests cover depths of submergence of 0.5 and 1.0 chords, vapor cavitation numbers from 0.06 to 2.34, and angles of attack from 3° to 15°. Data were obtained for the case of partial vapor cavitation as well as for the conditions of base ventilated and fully ventilated operation. In all of the cases, the trailing cavity was vented to atmospheric pressure through the cavity behind the blunt base of the parabolic, surface-piercing, vertical strut.

BuShips Parent Hydrofoil Model

The 5-in. chord BuShips parent hydrofoil model has a rectangular planform with an aspect ratio of 3- and 5-in. chord. Its cross section was obtained by assuming two terms in the pressure distribution expansion for the equivalent air-

Table 1 Ordinates of 5-in. chord model of BuShips parent hydrofoil

x, % c	x, in.	$-y_0$, % c	$-y_0$, in.	y_c, % c	y_c, in.	t, % c	t, in.
0	0	0	0	0	0	0	0
2.5	0.125	0.03	0.0015	0.53	0.0265	0.56	0.0280
5.0	0.250	0.04	0.0020	0.84	0.0420	0.88	0.0440
7.5	0.375	0.07	0.0035	1.15	0.0575	1.22	0.0610
10.0	0.500	0.08	0.0040	1.42	0.0710	1.50	0.0750
15.0	0.75	0.13	0.0065	1.94	0.0970	2.07	0.1035
20.0	1.00	0.17	0.0085	2.41	0.1205	2.58	0.1290
25.0	1.25	0.23	0.0115	2.91	0.1455	3.14	0.1570
30.0	1.50	0.28	0.0140	3.34	0.1670	3.62	0.1810
35.0	1.75	0.36	0.0180	3.76	0.1880	4.12	0.2060
40.0	2.00	0.45	0.0225	4.19	0.2095	4.64	0.2320
45.0	2.25	0.57	0.0285	4.63	0.2315	5.20	0.2600
50.0	2.50	0.72	0.0360	5.04	0.2520	5.76	0.2880
55.0	2.75	0.90	0.0450	5.44	0.2720	6.34	0.3170
60.0	3.00	1.10	0.0550	5.82	0.2910	6.92	0.3460
65.0	3.25	1.34	0.0670	6.22	0.3110	7.56	0.3780
70.0	3.50	1.61	0.0805	6.59	0.3295	8.20	0.4100
75.0	3.75	1.92	0.0960	6.98	0.3490	8.90	0.4450
80.0	4.00	2.28	0.1140	7.36	0.3680	9.64	0.4820
85.0	4.25	2.69	0.1345	7.75	0.3875	10.44	0.5220
90.0	4.50	3.14	0.1570	8.12	0.4060	11.20	0.5630
95.0	4.75	3.65	0.1825	8.49	0.4245	12.16	0.6070
100.0	5.00	4.21	0.2105	8.85	0.4425	13.06	0.6530

Presented as Preprint 64-308 at the 1st AIAA Annual Meeting, Washington, D. C., June 29–July 2, 1964; revision received November 30, 1964. This research was sponsored by the Bureau of Ships, U. S. Navy, under Contract No. NObs-88164. The material has been published for limited circulation as part of a Hydronautics, Inc. report.[1] The permission of BuShips to submit it for publication by AIAA is gratefully acknowledged.

* Associate Research Scientist.
† Research Scientist.

foil in the linearized theory for supercavitating hydrofoils operating near a free surface.[1, 3] The foil was designed for operation at a depth of 1 chord, has a camber of 0.0875, a design angle of attack of 2.5°, and no quasi-parabolic thickness (i.e., $\tau = 0$).[3] In addition, the foil has a built-in induced curvature correction that consists of an added circular arc camber/chord of 0.0099.

The foil is supported by a single parabolic strut with the same chord as the foil and a maximum thickness of 15% of its chord. Strut and foil are both constructed of stainless steel. Figure 1 is a photograph of the foil and Fig. 2 shows its cross section. The coordinates of the section are given in Table 1.

Apparatus and Procedure

High-Speed Water Channel

The tests were conducted in the high-speed water channel at Hydronautics, Inc. This is a free-surface, circulating, variable-pressure water channel, which facilitates the simultaneous scaling of free-surface effects and cavitation number. Figure 3 shows the foil in supercavitating flow and Fig. 4 is a schematic drawing of the channel arrangement.

The test section is 2 ft wide and 12 ft long with a bottom slope of 1 in. in 12 ft. A sluice gate at the entrance of the test section allows the water depth to be varied from about 6 in. to 2 ft.

The air pressure above the water can be lowered from 1 atm to slightly less than $\frac{1}{10}$ atm, whereas the water temperature can be held constant at any desired level between 70° and 120°F. A detailed description of the channel is contained in Ref. 6.

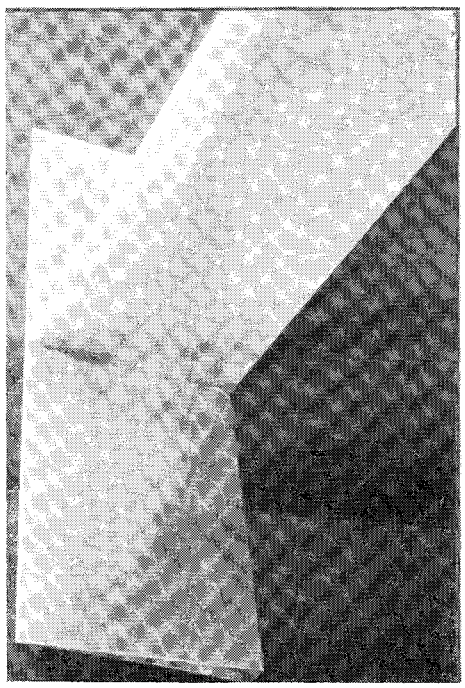

a)

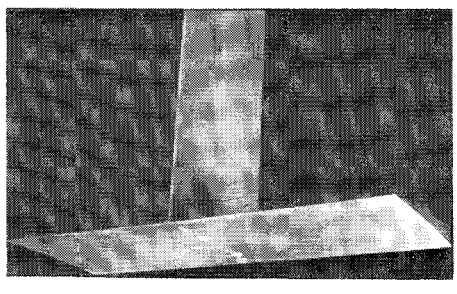

b)

Fig. 1 The 5-in. chord model of the BuShips parent supercavitating hydrofoil.

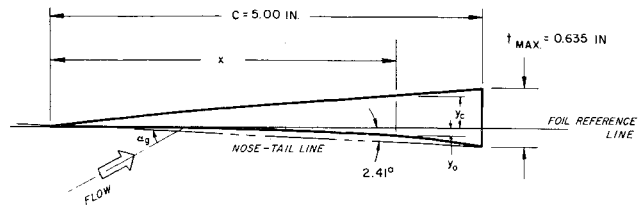

Fig. 2 Section of 5-in. chord model of BuShips parent hydrofoil.

Instrumentation

The strut supporting the foil is connected through a clevis to a truss-construction model-support beam, which is located under the test-section cover. This arrangement is shown schematically in Fig. 5. Each end of the beam is supported by a piston going through the test-section cover. The pistons are in turn connected to cranks on a common shaft and set 180° out of phase. By rotating this shaft, the beam can be tilted to 5° on either side of horizontal, thus allowing a total change in angle of attack of 10°. With the beam horizontal, the hydrofoil is set in the clevis at an initial geometric angle of attack α_g', uncorrected for wall effects, of about 7.5°. Thus the range of α_g' which can be tested without resetting the initial angle is from 2.5° to 12.5°.

Four variable reluctance block gages are used to measure the forces on the model. At each end of the beam, one pair of gages forms the junction between the beam and the supporting pistons. One of these is oriented so as to measure forces in a direction parallel to the beam, the other so as to measure normal forces. The output of each gage is fed to an amplifier and is then digitized and displayed on a counter. The forces thus indicated are then resolved into lift and drag, perpendicular and parallel to the direction of the flow.

The water speed in the test section is determined with a water-mercury manometer, which reads the difference in static pressure across the contraction located upstream of the test section. These manometer readings have been calibrated against pitot-static surveys to give test section velocities at various water depths throughout the test range. The ambient channel pressure is read with a mercury barometer and the water depth is read from a scale on the test section window 3 ft upstream from the leading edge of the foil.

Test Procedure

The foil was tested at depth/chord ratios of 0.5 and 1.0 and at speeds varying from 30 to 52 fps. These speeds gave

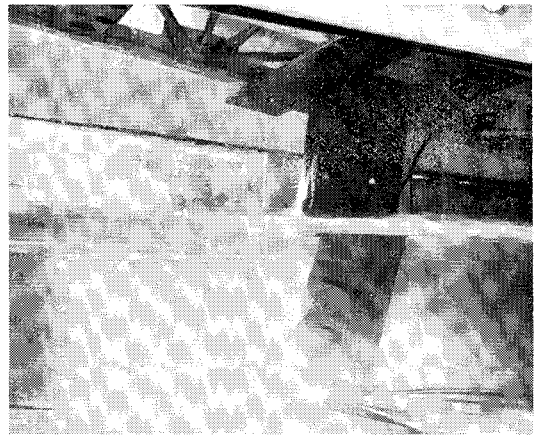

Fig. 3 The model in fully ventilated flow.

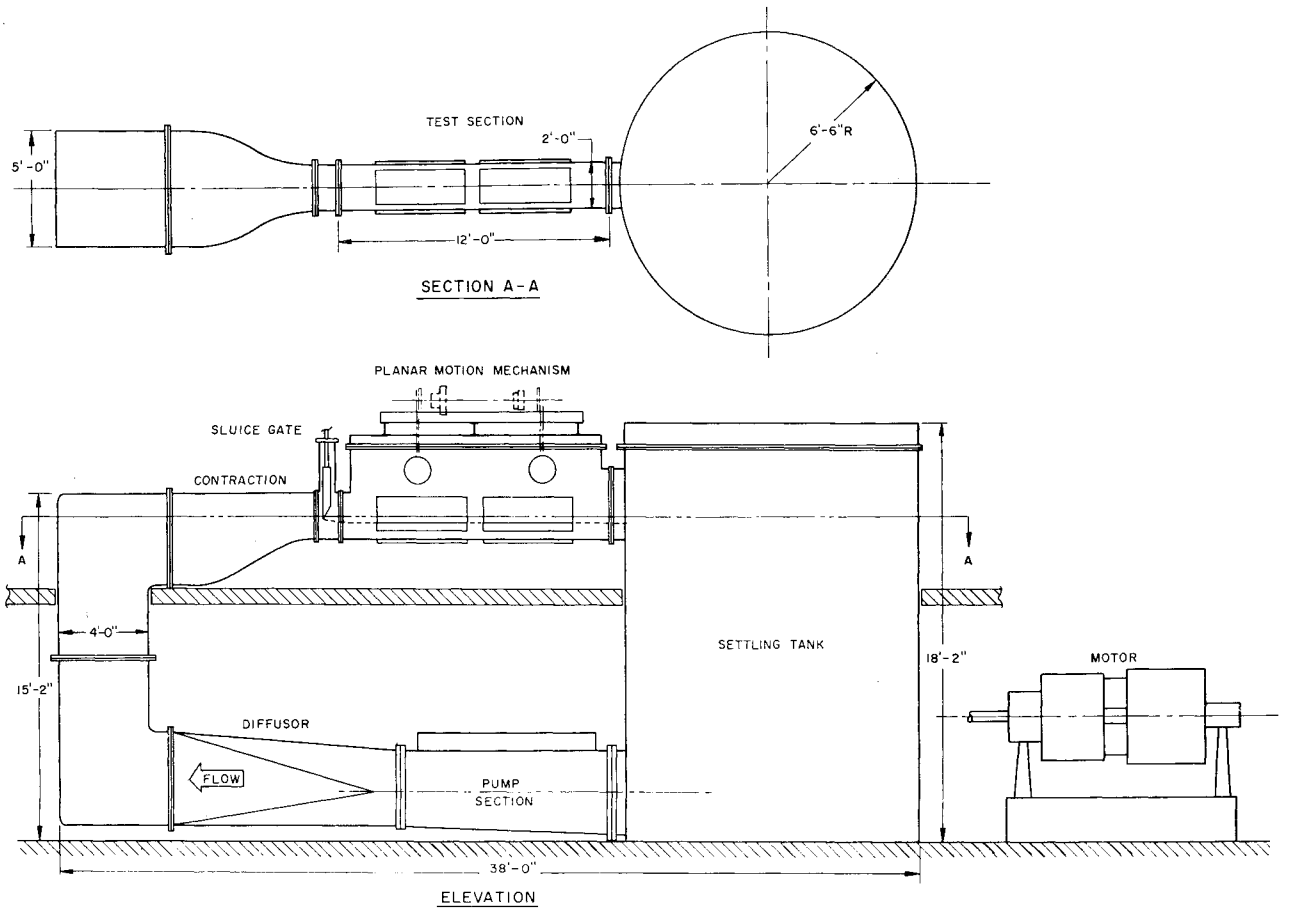

Fig. 4 Variable-pressure, free-surface, high-speed channel (schematic).

Froude and Reynolds numbers, based on the foil chord, from 8.1 to 14.3 and from 1.4 × 10^6 to 2.6 × 10^6, respectively. The ambient pressure was varied from 1 atm to about $\frac{1}{10}$ atm while the water temperature was held between 80° and 100°F. This yielded vapor cavitation numbers between 0.06 and 2.34.

The geometric angle of attack α_g', uncorrected for wall effects, was varied from 2.5° to 12.5° while the depth of submergence was held constant. In the majority of tests, α_g' was varied in 1° increments. However, because of the presence of hysteresis on the ventilation inception angle, some data were taken by first increasing the angle of attack until ventilation occurred, and then decreasing the angle until the foil again became wetted on its upper surface. In these tests, the angle of attack was varied in $\frac{1}{4}$° increments in the neighborhood of the hysteresis loop.

Wall Effects and Data Reduction

The conditions under which the model is tested in the water channel are not the same as those in open water. The presence of the channel walls and bottom influences the flow pattern and must be accounted for if the data are to represent the foil performance in open water. The corrections result from two sources: 1) the image of the bound and trailing vortex system in the walls and bottom; and 2) the "blockage" caused by the finite thickness of the model and cavity, that is, the image of the thickness source and sink system in the walls and bottom.

1) The image vortex system causes an induced upwash, which has the effect of making the measured angle of attack and the measured drag too small. The correction for this effect is the same as that used in wind tunnels and is outlined in Chap. 6 of Ref. 7.

2) The blockage from the finite size of the model and cavity causes induced velocities in all three coordinate directions.

a) There is an induced upwash that has the same effect as that caused by the image vortex system. Ho's[8] linearized theory for a two-dimensional, supercavitating flat plate in shallow water provides the necessary information for a bottom correction due to the cavity size. Ho's results have been rewritten in terms of cavity drag coefficient so that the corrections derived for a flat plate may be used to approximate the corrections for a cambered foil. This is possible because the upwash is a function of cavity size, which is dependent on the cavity drag. Since the drag of a cambered foil at a given lift coefficient is less than the drag of a flat plate at the same lift coefficient, the cambered foil would be less influenced by the proximity of the bottom. A small correction is applied to the results of the two-dimensional theory to account for finite aspect ratio. Since the strut cavity thickness is small, its effect on upwash is negligible and is not considered.

b) An induced inwash is caused in the same manner as the induced upwash. Since this inwash is symmetrical about the test section vertical centerplane and is in a spanwise direction, it was felt that it would not materially influence the results and could be neglected.

Table 2 Estimated accuracy of measured quantities

Lift, lb (400 lb maximum)	±2.0
Drag, lb (75 lb maximum)	±0.5
Angle of attack, deg	±0.1
Depth of submergence, in.	±0.2
Channel pressure, ft of water head	±0.1
Mean water temperature, °F	±0.5
Maximum deviation from mean water temperature, °F	±3.0

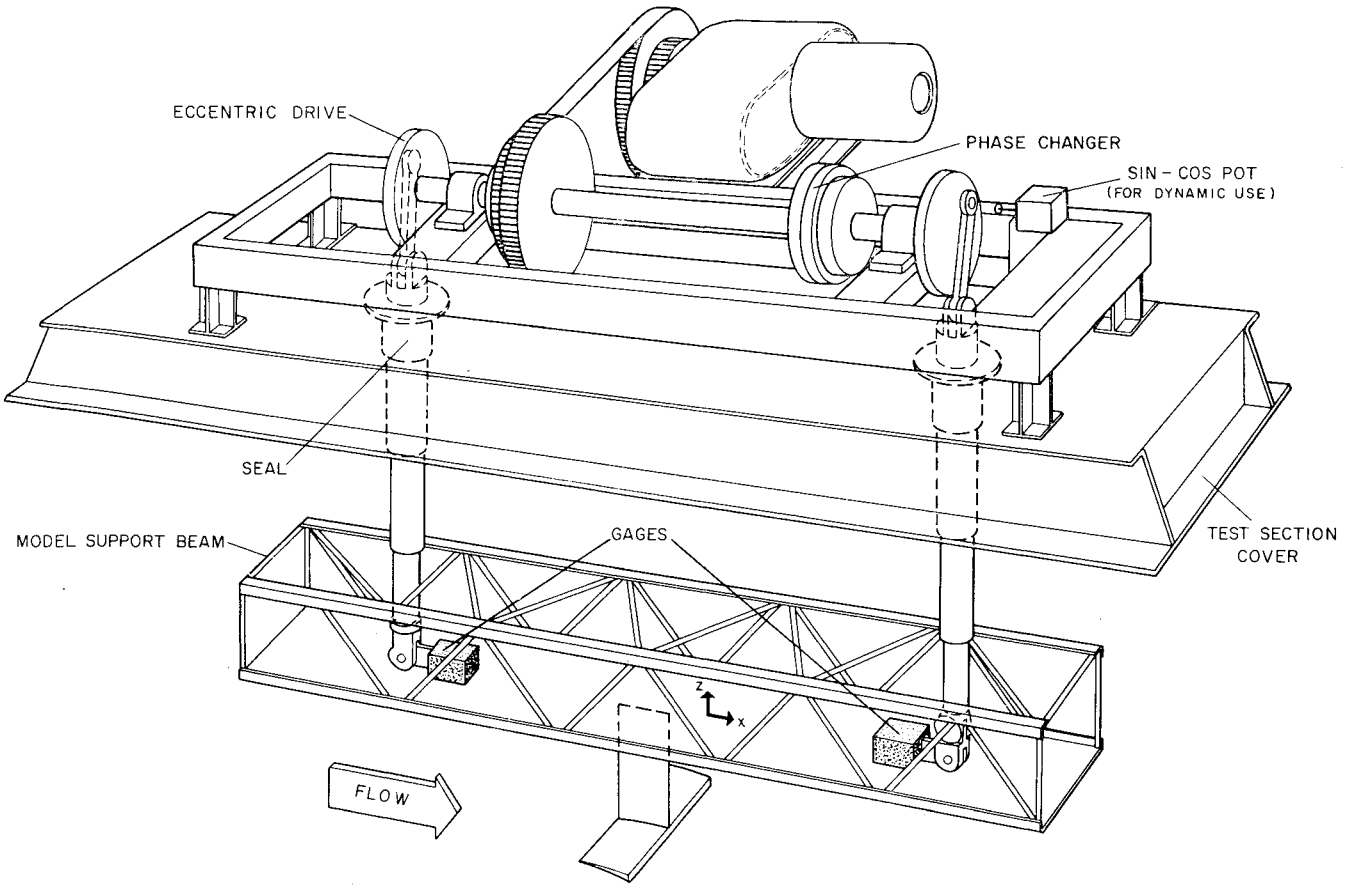

Fig. 5 Schematic of foil mounted on model support beam showing location of block gages and direction of forces.

c) There also exists an induced velocity in the direction of flow. This has the same effect as increasing the dynamic pressure thus making the measured force coefficients too large. Since this correction is small, its magnitude was obtained approximately by using a modification of the correction used for closed throat wind tunnels.

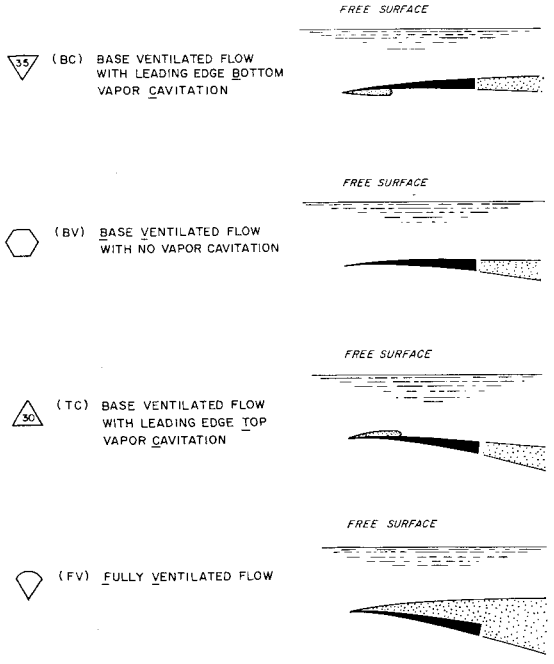

Fig. 6 Schematic representations of flow regimes with the symbols and abbreviations used to identify them in the data presentation.

The data reduction and boundary corrections were carried out on an IBM 1620 computer. It was found that the maximum corrections occurred at high angles of attack and amounted to a decrease in lift and drag coefficients of 15% at an angle of attack of 12.4° and a depth/chord ratio of 1.0. Figure 6 gives definitions of the symbols used in Figs. 7 and 8, which show samples of corrected and uncorrected data.

Accuracy

The data in this report are compiled from some 350 test runs conducted at various times between November 27, 1962 and March 10, 1964. During this time, several modifications and improvements were made in the test equipment, yet it was found that tests were being duplicated without difficulty. For tests reported herein the accuracy of the measured quantities is estimated to be within the limits shown in Table 2.

Results and Discussion

The lift and drag coefficients are those for the complete strut and foil configuration treated as a unit but are nondimensionalized by using the projected area of the foil only. These coefficients, corrected for the effects of the channel walls, were first plotted against vapor cavitation number. Cross-plots were then made to obtain the dependence of lift coefficient, drag coefficient, and lift/drag ratio on geometric angle of attack. These cross-plots were made for four values of vapor cavitation number σ_v = 2.0, 1.0, 0.50, 0.25 and two depths of submergence h/c = 1.0, 0.50 and are included as Figs. 9–14. Lines were drawn through the base ventilated data, and NASA theory for zero cavity cavitation number σ_c is included for purposes of comparison with the fully ventilated data. The theory includes the strut drag and a skin-friction coefficient of 0.003.

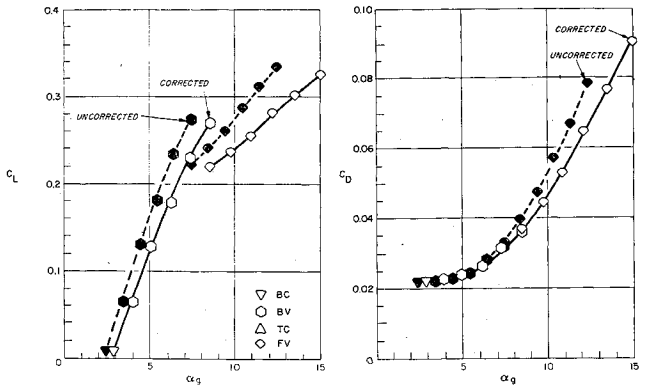

Fig. 7 Sample of corrected and uncorrected data showing effect of wall concentrations on the variation of lift and drag coefficients with geometric angle of attack, depth/chord ratio = 1.0.

Flow Regimes

It is important to note the different flow regimes that occur in the operation of the foil because they have a crucial effect on foil performance and are essential in obtaining a useful understanding of experimental results. Figure 6 depicts the flow regimes occurring in these tests and defines the symbols and abbreviations used to identify them in the data plots. Figure 15 shows their dependence on σ_v and angle of attack.

At low angles of attack, the foil is base ventilated with leading edge vapor cavitation on the bottom surface. This vapor cavitation is greatest directly under the strut and increases with decreasing values of σ_v and decreasing angles of attack. Fluctuations in the portion of the foil covered by vapor cavitation cause some fluctuation in the forces measured and contribute to data scatter in this regime. As the angle of attack is increased, the bottom cavitation disappears and the force readings become steady. At still higher incidence, leading edge vapor cavitation occurs on the upper surface. This cavitation also increases with decreasing σ_v and, of course, also with increasing angle of attack. As before, fluctuations in the extent of the cavitation cause fluctuations in the forces measured in this flow regime, and thus contribute to data scatter.

The values of incipient cavitation number show considerable scatter, and thus the regions of incipient cavitation are not well defined. This situation is primarily the result of difficulty encountered in attempting to visually detect the presence of incipient cavitation.

As the angle is further increased the foil becomes fully ventilated on its upper surface. A hysteresis loop is observed in the incipient ventilation angle. That is, if the foil is base ventilated and the angle increased, it becomes fully ventilated at some angle, say α_1. If the angle is then decreased, the foil would remain fully ventilated until it reached some lower angle $\alpha_2(\alpha_1 > \alpha_2)$. Thus, in the range of angles between α_2

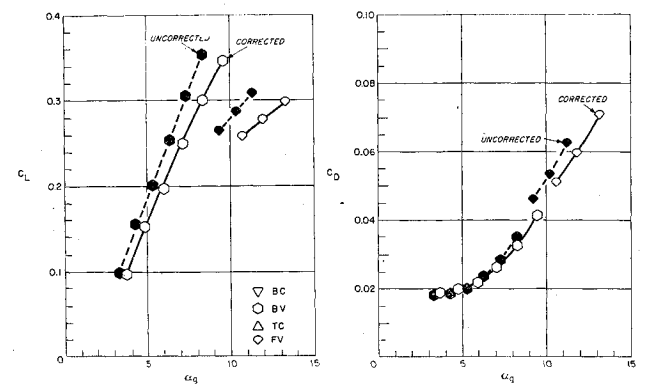

Fig. 8 Sample of corrected and uncorrected data showing effect of wall corrections on the variation of lift and drag coefficients with geometric angle of attack, depth/chord ratio = 0.5.

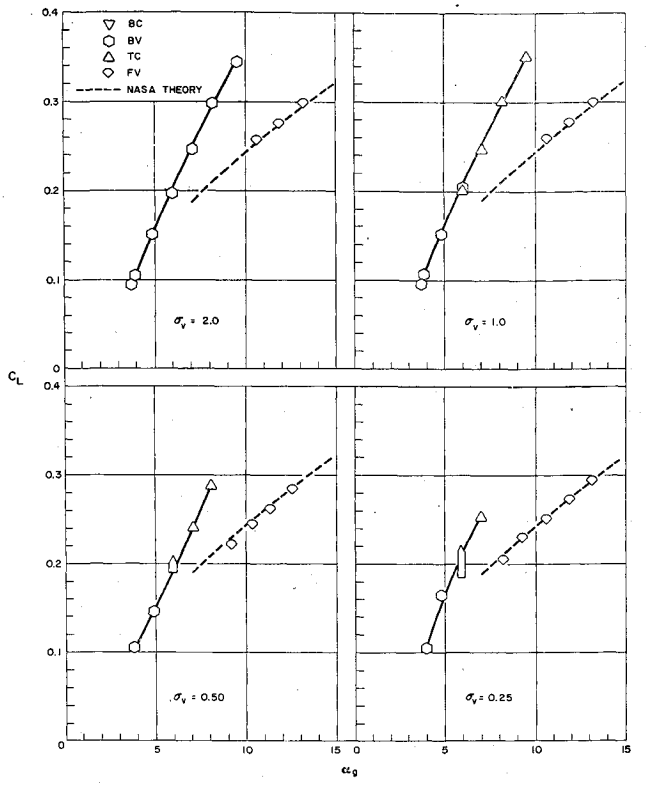

Fig. 9 Variation of lift coefficient with geometric angle of attack for various values σ_v, depth/chord ratio = 0.5.

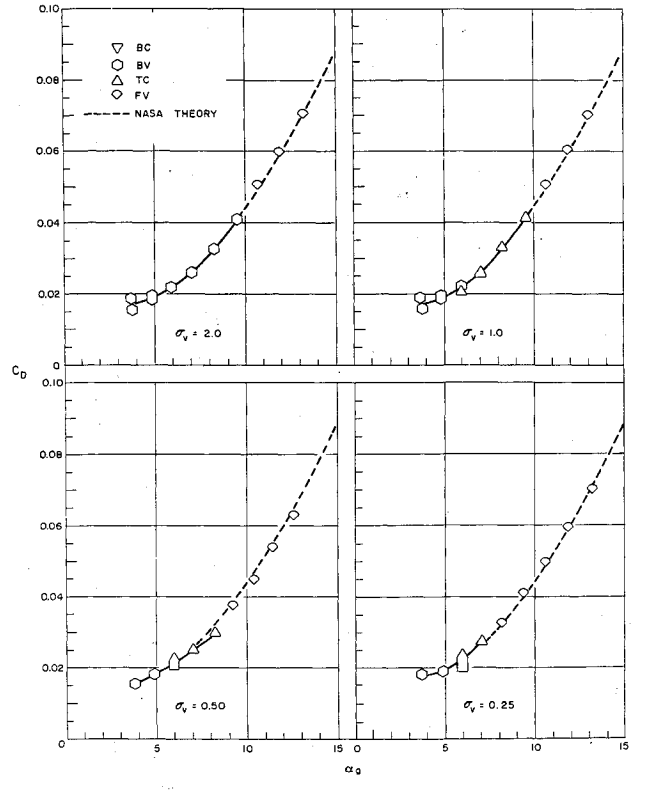

Fig. 10 Variation of drag coefficient with geometric angle of attack for various values of σ_v, depth/chord ratio = 0.50.

and α_1, either base ventilated flow or fully ventilated flow can exist. On several occasions the foil was base ventilated on one end and fully ventilated on the other end with the strut forming a barrier between the two flow regimes. (Data were not recorded under these conditions.) The amount of hysteresis decreased with decreasing values of σ_v and depth of submergence.‡

In all cases the trailing cavity was vented to atmospheric pressure through the cavity behind the strut. Measurements of the cavity pressure made in the early stages of the test program showed that the cavity pressure was nearly atmospheric. Cavitation number σ_c had maximum values of 0.04.

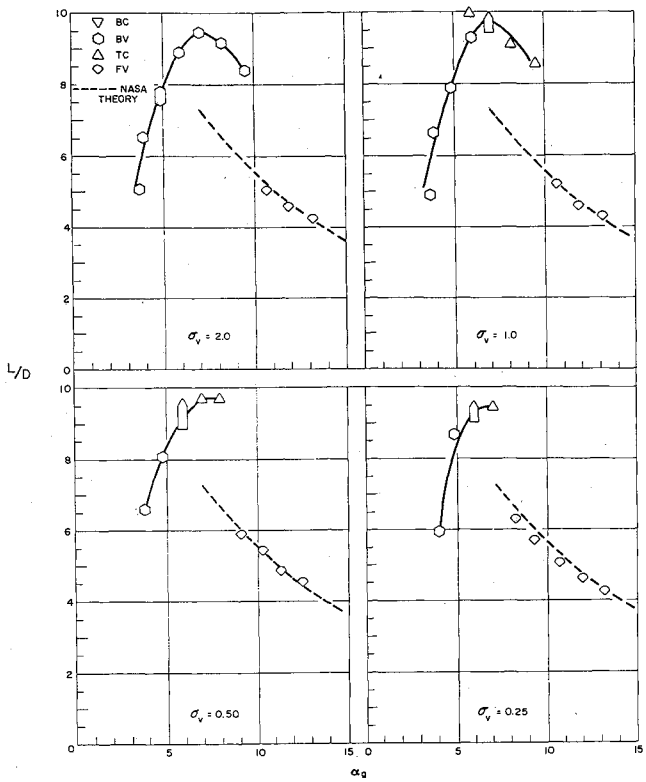

Fig. 11 Variation of lift/drag ratio with geometric angle of attack for various values of σ_v, depth/chord ratio = 0.50.

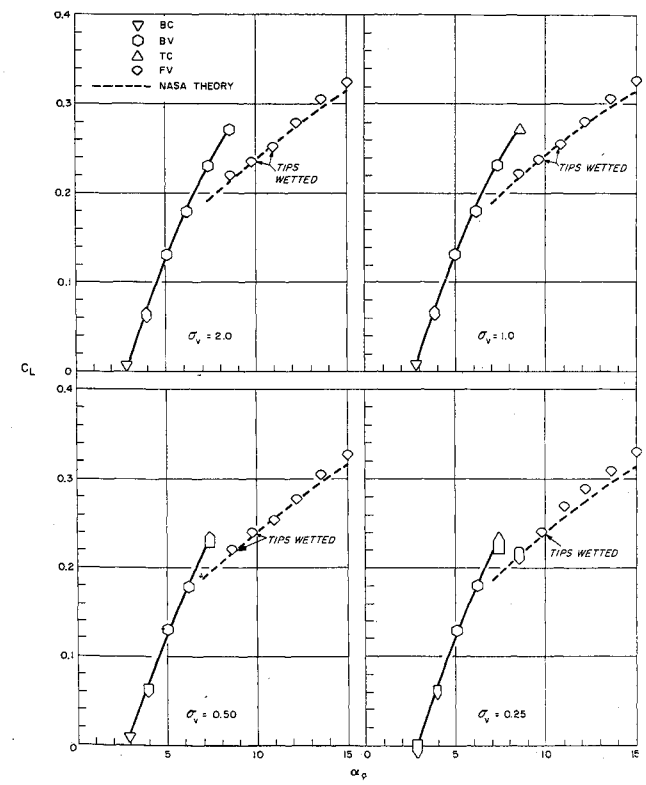

Fig. 12 Variation of lift coefficient with geometric angle of attack for various values of σ_v, depth/chord ratio = 1.0.

Lift and Drag Data

Figures 9 and 12 showing the variation of C_L with α_g exhibit the typical drop in lift which occurs when the foil becomes fully ventilated. This drop in lift is the result of an increase in pressure over the upper surface of the foil as compared to the pressure that exists when the foil is base ventilated. It is interesting to note that there is no change in drag when the foil becomes fully ventilated (see Figs. 10 and 13). An examination of the data showed that, the reduction in induced drag that occurs when the lift drops, was just offset by the increase in cavity drag that occurs in the fully ventilated condition. This is peculiar of this particular section, planform, and aspect ratio, and in general there would be a discontinuity in the drag curve depending on the relative magnitudes of induced and cavity drag.

The transition between base ventilated and fully ventilated flow occurs in three different ways that can be roughly divided according to vapor cavitation number: 1) σ_v greater than 1.8, 2) σ_v between 1.8 and 0.1, and 3) σ_v less than 0.1.

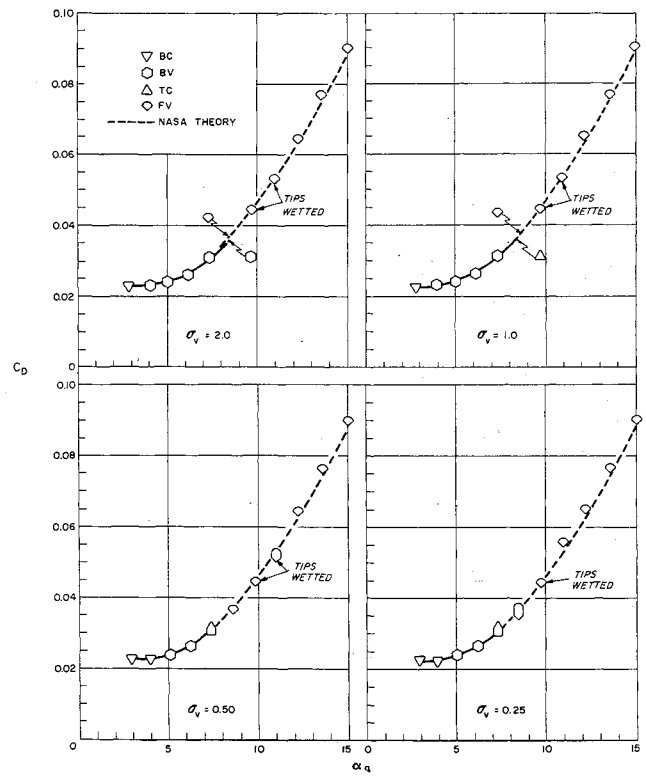

Fig. 13 Variation of drag coefficient with geometric angle of attack for various values of σ_v, depth/chord ratio = 1.0.

‡ A qualitative, experimental investigation was conducted at Hydronautics, Inc., into means of eliminating ventilation hysteresis. It was found that, by using appropriately designed pods and/or fences or notches on the strut, it is possible to eliminate the hysteresis loop and obtain ventilated flow at the lower end of the previously existing loop, i.e., at α_2. The principle of the techniques used was to provide natural ventilation paths to the leading edge of the foil. It is quite clear that the detailed design of such devices depends on the particular requirements of a given wing-pod-strut system.

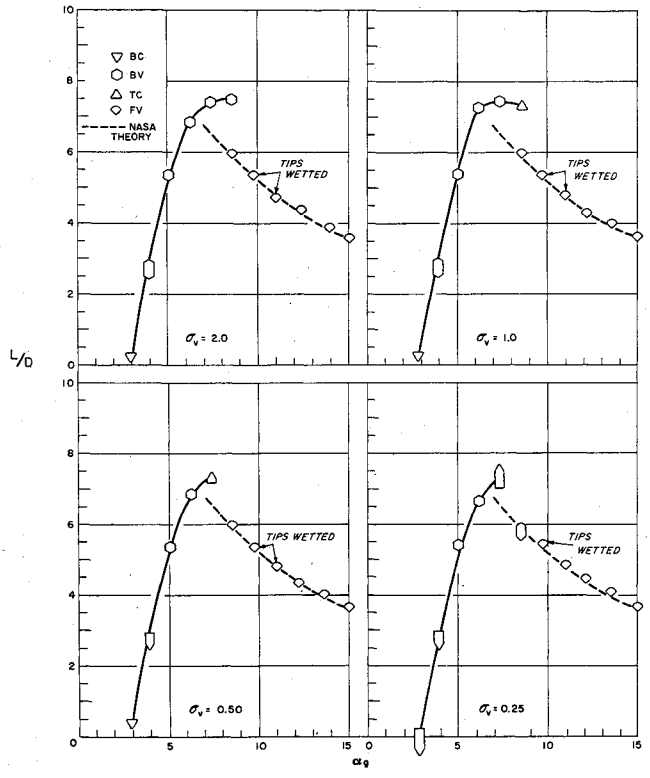

Fig. 14 Variation of lift/drag ratio with geometric angle of attack for various values of σ_v, depth/chord ratio = 1.0.

1) When σ_v is greater than 1.8, very little vapor cavitation takes place before full ventilation occurs. The foil remains base ventilated as the angle of attack is increased until it reaches a critical angle where it suddenly becomes fully ventilated and experiences a large loss in lift. This is the upper bound of the hysteresis loop. As the angle is again decreased, the upper cavity first collapses at the foil tips, with little change in lift, and then becomes base ventilated with an accompanying increase in lift. This is the lower bound of the hysteresis loop.

2) When σ_v is between 1.8 and 0.1, leading edge vapor cavitation occurs on the top of the foil before it becomes fully ventilated. At values of σ_v near 1.8, this cavitation may cover only a few percent of the chord before the foil becomes fully ventilated, and ventilation occurs at about the same angle as in the first case. As σ_v becomes lower, more vapor cavitation occurs, and when σ_v is near 0.1, as much as 30 to 40% of the chord may be covered by cavitation before the foil finally becomes fully ventilated. The cavitation is greatest about midway between the foil tips and the strut and is often very unsteady. The smaller the cavitation number the sooner the foil becomes fully ventilated. The hysteresis loop also becomes narrow as σ_v decreases. When σ_v approaches 0.1, the hysteresis loop virtually disappears. The transition from fully ventilated to base ventilated flow occurs in the same manner as when σ_v is large.

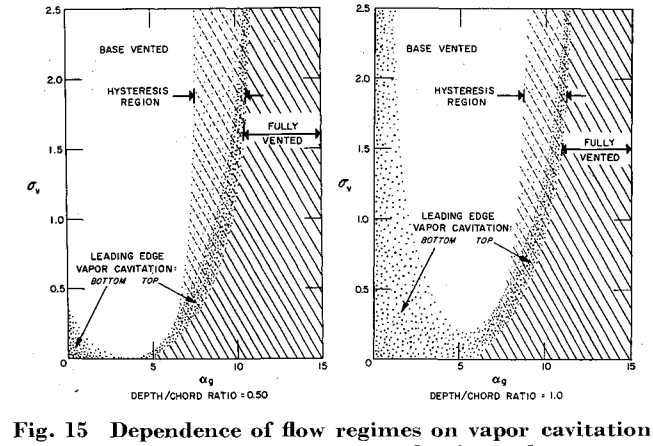

Fig. 15 Dependence of flow regimes on vapor cavitation number and geometric angle of attack.

3) At values of σ_v less than 0.1, there is no hysteresis (see Figs. 16 and 17). As the angle of attack is increased from a condition of base ventilated flow, a small amount of leading edge vapor cavitation appears on the upper surface of the foil. As the angle is increased further, the foil becomes ventilated in narrow strips on its upper surface about half-way between the tips and the strut. These strips grow and merge into a single band of ventilated flow on each side of the foil leaving only the tips and root base ventilated. Finally the whole foil becomes fully ventilated. The process is continuous and there is no sudden loss in lift. When the angle of attack is decreased, the reverse procedure takes place.

Figures 16 and 17 contain data taken at low values of σ_v in the vicinity of the transition between base ventilated and fully ventilated flow. They show that, at low vapor cavitation number, the drop in lift associated with ventilation is small and does not occur suddenly.

It can be shown that the hysteresis loop is also dependent on aspect ratio: when full ventilation occurs with its corresponding drop in lift, the induced downwash is also reduced. Thus for a given geometric angle of attack, the foil effectively sees a higher angle of attack when fully ventilated than when base ventilated. The geometric angle of attack must then be reduced until the effective angle of attack becomes small enough for the foil to again become base ventilated. When this occurs, the lift, and thus the downwash, increase; thus the effective angle of attack is further reduced.

Since the induced downwash is inversely proportional to aspect ratio, the previous reasoning would lead one to expect large hysteresis loops for foils of small aspect ratio. This has in fact been observed on tests of other foils. For example, a flat plate with an aspect ratio of one had a hysteresis loop over a range of 5°, whereas a similar foil with an aspect ratio of 3 only had hysteresis over a 1° range in angle of attack. These tests, not yet published, were also conducted in the high-speed channel at Hydronautics, Inc.

Comparison of Theory and Experiment

The broken line in Figs. 9–14 shows the hydrodynamic performance of the BuShips hydrofoil as predicted by the NASA theory for $\sigma_c = 0$.[2, 9] The theory applies only to the fully ventilated condition and should not be compared to data in the base ventilated region. The solid line through the base vented data is merely drawn through the data points and does not represent theory. A comparison between the measured lift curve slope in the base vented condition and that predicted by theory [Ref. 10, Eq. (48)] shows that the theoretical value is somewhat lower: at a depth/chord ratio of 1, the measured lift curve slope is 3.17 and the predicted value is 2.86, a difference of 10%. The theory (in the fully vented condition) is not corrected for finite cavitation number but does include the theoretical strut drag and a friction coefficient of 0.003.

The agreement between theory and experiment is very good indeed, especially if one considers the magnitude of the wall corrections. It is possible that the excellent agreement between theory and experiment shown here is unique for this particular model and may be the result of the large wall corrections required. Further comment on this question must await experimental results obtained in the channel on models of differing sizes.

At the design depth of 1 chord, the lowest angle at which ventilation could be obtained was 7.5° and occurred at the lowest vapor cavitation number 0.10 at which tests were conducted at this depth. Although this ventilation angle is

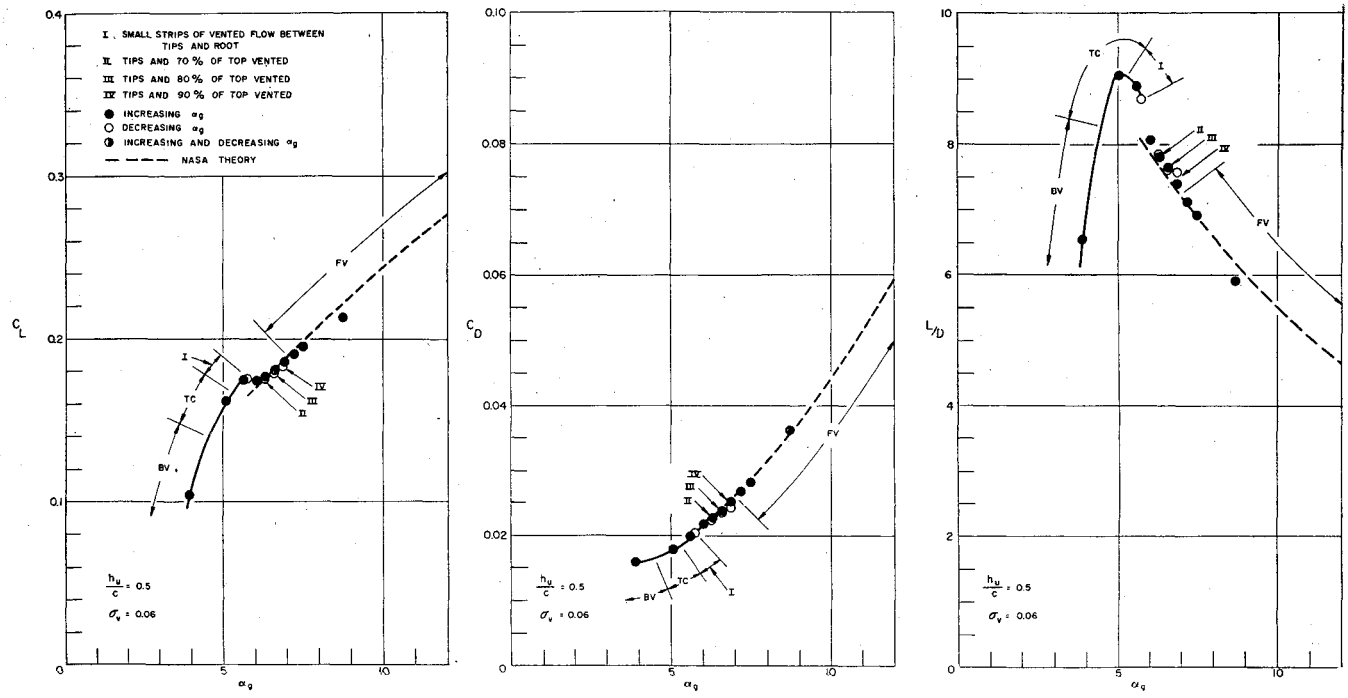

Fig. 16 Variation of lift and drag coefficients and lift/drag ratio with geometric angle of attack depth/chord ratio = 0.5, $\sigma_v = 0.06$.

higher than the 4.5° predicted by theory (see Fig. 17), it is much lower than the lowest ventilation angle reported by Conolly.[11] The lowest vapor cavitation number obtained in the present series of tests $\sigma_v = 0.06$ occurred at a depth of $\frac{1}{2}$ chord and under these conditions the ventilation angle was somewhat lower (6.3°, see Fig. 16) but it must be remembered that the ventilation angle can be expected to decrease with operating depth as well as with vapor cavitation number.

It is apparent that, as the vapor cavitation number decreases, the lower end of the ventilation inception hysteresis loop will approach the intersection of the fully ventilated and base ventilated lines on a plot of lift coefficient vs angle of attack (see Figs. 9 and 12). It was found that, at cavitation numbers typical of full-size craft ($\sigma_v = 0.10$ at 90 knots), the ventilation inception hysteresis disappeared and there was very little loss in lift when ventilation occurred.

It can be seen in Figs. 11 and 14 that when the foil is fully ventilated, the lift/drag ratio increases with decreasing angle of attack. These data confirm the theoretical prediction of the importance of operating fully ventilated at as low an angle as possible.

In the present experiments, at the lowest angle at which fully ventilated flow could be obtained, the lift/drag ratio of the foil-strut combination was 6.5 at a depth of 1 chord with

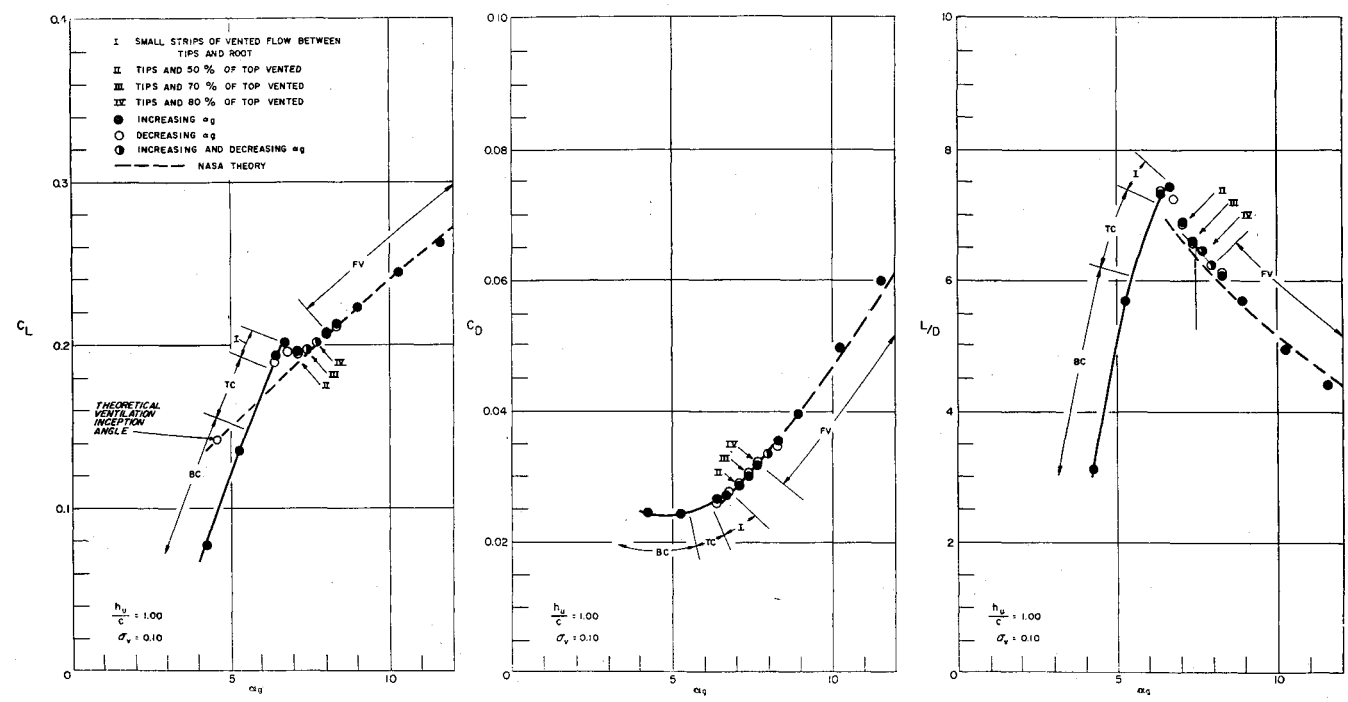

Fig. 17 Variation of lift and drag coefficients and lift/drag with geometric angle of attack, depth/chord ratio = 1.0, $\sigma_v = 0.10$.

$\sigma_v = 0.10$, and 7.8 at a depth of $\frac{1}{2}$ chord with $\sigma_v = 0.06$. These are, of course, maximum L/D values obtained in ventilated flow at the respective vapor cavitation numbers. It must be remembered, however, that this foil has neither an optimum section nor an optimum planform, and it is felt that higher lift/drag ratios than those obtained here can be reached with a supercavitating foil system of optimum design.

Conclusions

Conclusions based on the results of this experimental investigation are summarized as follows.

1) The agreement between theoretical and experimentally determined force coefficients for the BuShips hydrofoil is very good, especially in view of the magnitude of the wall corrections.

2) The ventilation inception hysteresis loop vanishes, and the ventilation inception angle approaches the intersection of the fully ventilated and base ventilated lines (on a plot of lift coefficient vs angle of attack) as the vapor cavitation number approaches zero.

3) At a depth of 0.5 chords, the maximum lift/drag ratio of the foil-strut combination when operating in a base ventilated condition is 10.0 and occurs at a vapor cavitation number of 1.0 and an angle of 6.0°. At high vapor cavitation numbers ($\sigma_v > 1.0$), the maximum lift/drag ratio when operating in a fully ventilated condition is 5.2 and occurs at an angle of 10.6°. At a vapor cavitation number of 0.06, the maximum lift/drag ratio in a fully ventilated condition is 7.8 and occurs at an angle of 6.3°.

4) At a depth of 1.0 chord, the maximum lift/drag ratio of the foil-strut combination when operating in a base ventilated condition is 7.5 and occurs at a vapor cavitation number of 2.0 and an angle of 8.5°. At high vapor cavitation numbers ($\sigma_v > 1.0$), the maximum lift/drag ratio when operating in a fully ventilated condition is 6.0 and occurs at an angle of 8.5°. At a vapor cavitation number of 0.10, the maximum lift/drag ratio in a fully ventilated condition is 6.5 and occurs at an angle of 7.5°.

References

[1] Scherer, J. O. and Auslaender, J., "Experimental investigation of the 5-inch chord model of the BuShips parent supercavitating hydrofoil," Hydronautics, Inc., TR 343-1 (March 1964).

[2] Auslaender, J., "The linearized theory for supercavitating hydrofoils operating at high speed near a free surface," Hydronautics, Inc., TR 001-5 (June 1961).

[3] Auslaender, J., "Design charts for one and two strut supercavitating hydrofoil wings," Hydronautics, Inc., TR 001-8 (October 1961).

[4] Auslaender, J., "Low drag supercavitating hydrofoil sections," Hydronautics, Inc., TR 001-7 (1962).

[5] Tulin, M. P. and Burkhart, M. P., "Linearized theory for flows about lifting foils at zero cavitation number," David Taylor Model Basin Rept. C-638 (1955).

[6] Johnson, V. E. and Goodman, A., "The Hydronautics, Incorporated variable-pressure, free-surface, high-speed channel," Hydronautics, Inc., TR 229-1 (1964).

[7] Pope, A., *Wind Tunnel Testing* (John Wiley and Sons, Inc., New York, 1954).

[8] Ho, H. T., "Linearized theory for a supercavitating hydrofoil operating in a fluid of finite depth," Hydronautics, Inc., TR 119-7 (1963).

[9] Johnson, V. E., "Theoretical and experimental investigation of supercavitating hydrofoils operating near the free-water surface," NASA TR R-93 (1961).

[10] Martin, M., "The stability derivatives of a hydrofoil boat," Hydronautics, Inc., TR 001-10 (1963).

[11] Conolly, A. C., "Experimental investigation of supercavitating hydrofoils with flaps," General Dynamics, Convair, GDC-63-210 (1963).